PLOS COMPUTATIONAL BIOLOGY

RESEARCH ARTICLE

A spectrum of routing strategies for brain networks

Andrea Avena-Koenigsberger[1]*, Xiaoran Yan[2], Artemy Kolchinsky[3], Martijn P. van den Heuvel[4,5], Patric Hagmann[6], Olaf Sporns[1,2]

1 Department of Psychological and Brain Sciences, Indiana University, Bloomington, IN, United States of America, **2** IU Network Institute, Indiana University, Bloomington, IN, United States of America, **3** Santa Fe Institute, Santa Fe, NM, United States of America, **4** Connectome Lab, Complex Trait Genetics, Department of Neuroscience, Center for Neurogenomics and Cognitive Research, Amsterdam Neuroscience, VU Amsterdam, **5** Department of Clinical Genetics, Amsterdam University Medical Center, Amsterdam, The Netherlands, **6** Department of Radiology, Centre Hospitalier Universitaire Vaudois (CHUV) and University of Lausanne (UNIL), Lausanne, Switzerland

* aiavenak@indiana.edu

Check for updates

OPEN ACCESS

Citation: Avena-Koenigsberger A, Yan X, Kolchinsky A, van den Heuvel MP, Hagmann P, Sporns O (2019) A spectrum of routing strategies for brain networks. PLoS Comput Biol 15(3): e1006833. https://doi.org/10.1371/journal.pcbi.1006833

Editor: Saad Jbabdi, Oxford University, UNITED KINGDOM

Received: August 17, 2018

Accepted: January 30, 2019

Published: March 8, 2019

Copyright: © 2019 Avena-Koenigsberger et al. This is an open access article distributed under the terms of the Creative Commons Attribution License, which permits unrestricted use, distribution, and reproduction in any medium, provided the original author and source are credited.

Data Availability Statement: All data files are available from the corresponding authors Github repository: https://github.com/aiavenak/lambda_spectrum.

Funding: OS was supported by the National Institutes of Health (R01-AT009036). PH was supported by the Leenaards Foundation. MPvdH was supported by a NWO-VIDI (452-16-015) and ALW open (ALWO.179) of the Netherlands Organisation for Scientific Research and a MQ

Abstract

Communication of signals among nodes in a complex network poses fundamental problems of efficiency and cost. Routing of messages along shortest paths requires global information about the topology, while spreading by diffusion, which operates according to local topological features, is informationally "cheap" but inefficient. We introduce a stochastic model for network communication that combines local and global information about the network topology to generate biased random walks on the network. The model generates a continuous spectrum of dynamics that converge onto shortest-path and random-walk (diffusion) communication processes at the limiting extremes. We implement the model on two cohorts of human connectome networks and investigate the effects of varying the global information bias on the network's communication cost. We identify routing strategies that approach a (highly efficient) shortest-path communication process with a relatively small global information bias on the system's dynamics. Moreover, we show that the cost of routing messages from and to hub nodes varies as a function of the global information bias driving the system's dynamics. Finally, we implement the model to identify individual subject differences from a communication dynamics point of view. The present framework departs from the classical shortest paths vs. diffusion dichotomy, unifying both models under a single family of dynamical processes that differ by the extent to which global information about the network topology influences the routing patterns of neural signals traversing the network.

Author summary

Brain network communication is typically approached from the perspective of the length of inferred paths and the cost of building and maintaining network connections. However, these analyses often disregard the dynamical processes taking place on the network and the additional costs that these processes incur. Here, we introduce a framework to study communication-cost trade-offs on a broad range of communication processes

Fellowship Data were provided (in part) by the Human Connectome Project, WU-Minn Consortium (Principal Investigators: David Van Essen and Kamil Ugurbil; 1U54MH091657) funded by the 16 NIH Institutes and Centers that support the NIH Blueprint for Neuroscience Research; and by the McDonnell Center for Systems Neuroscience at Washington University. The funders had no role in study design, data collection and analysis, decision to publish, or preparation of the manuscript.

Competing interests: The authors have declared that no competing interests exist.

modeled as biased random walks. We control the system's dynamics that dictates the flow of messages traversing a network by biasing node's routing strategies with different degrees of "knowledge" about the topology of the network. On the human connectome, this framework uncovers a spectrum of dynamic communication processes, some of which can achieve efficient routing strategies at low informational cost.

Introduction

The function of many real world complex networks is to relay information within and between their constituent elements. Efficient communication, i.e. the passing of information at high speed and high reliability at low cost to the system, is essential to the functioning of systems in many domains, ranging from technological to social and biological applications. For example, communication is central to the operation of brain networks, as it is necessary for information integration and for distributed neural computation [1]. However, the mechanisms that enable information to flow efficiently among large numbers of distributed elements interacting through a complex topology remain mostly unexplained.

Previous work on optimal routing in networks highlighted the importance of small-world topologies for promoting short communication pathways at low wiring cost [2,3]. Indeed, information transfer that takes place through topologically shortest paths is both fast and direct, and reduces a message's vulnerability to errors and attack [4]. Yet, such a communication model also has disadvantages: it discounts the vast majority of a network's structural connections [5,6], it is prone to bottlenecks and congestion [7–9], and it lacks robustness to edge failures [10]. Most importantly, a system's ability to route along shortest paths relies on all of the system's elements having information about the global topology of the network [11,12]. Therefore, an explicit analysis of the costs and benefits of efficient communication should take into account the cost associated with having access to global information, in addition to better-known costs such as wiring and energy consumption [1,13–17]. We refer to the cost of the information necessary for signal routing as the *informational cost*.

A drastically different picture emerges if we discard the premise that the system's elements are capable of accessing information about the global topology of the network. Under this scenario, signals are dispersed according to a random walk or diffusion process [18–21], driven only by local topological properties. While diffusion has no associated cost of storing global topological information, communication is inefficient if measured in terms of the time needed for a signal to arrive at a specific destination. This results in increased vulnerability to signal corruption and slower integration of information as signals are broadcast and spread indiscriminately across the network.

While shortest paths and diffusion have been extensively studied in the context of network communication, they merely represent the extremes of a spectrum of communication processes that deserve greater attention. As an example, for some types of network topologies, a preferential choice policy where messages are preferentially routed towards high degree nodes [22, 23] decreases search times significantly compared to random walks, yet the informational cost is small since nodes only need to "know" the degree of their neighbors. Brain networks are a case in point: on average, shortest paths tend to follow a low-to-high and then high-to-low degree sequence [24] and closeness centrality sequence [25], suggesting that efficient routing patterns in brain networks could be driven by a mixture of degree and closeness preferential choice policies. Preferential policies are often modeled as biased random walks [26], where the motion of a random walker located at a given node is biased according to an attribute (e.g.

degree) associated with the neighboring nodes. It has been shown that biased random walks can generate relatively efficient communication processes (high speed, low cost) and are able to account for navigation rules that are observed in real world systems [27–30], offering alternative interpretations of node centralities and community structures [31].

Here, we focus on a specific family of biased random walks, governed by routing strategies generated by a stochastic model that combines local and global information about the network topology. This framework allows us to explore a continuous spectrum of dynamics that converge onto shortest-path communication processes at one extreme, and random-walk (diffusion) communication processes at the other extreme. Therefore, under the presented framework, we unify a variety of communication models under a single family of dynamical processes, allowing us to investigate *communication cost* from a dynamic point of view in large-scale brain networks. For brain networks, the implications are that the extent to which brain regions can be characterized as highly efficient or central, is dependent upon the assumptions under consideration, here instantiated by a single parameter that controls the extent to which knowledge about the global network topology shapes the dynamics. With this framework we explore a family of communication models that have not been previously explored in the context of brain communication, and postulate that future investigations of brain communication dynamics should take into consideration the impact that functional demands and the availability of metabolic resources may have on the repertoire of routing patterns taking place on the network.

A continuous spectrum of routing strategies combining local and global information

We model messages or signals transferred from a source brain region to a target brain region as random walkers traversing a brain network, where network nodes and edges represent small cortical parcels that are connected by bundles of axons. We consider the dynamics of such random walkers (signals/messages) on the network, where walkers must reach an a priori specified target node t. Formally, let $\mathbf{X}$ be a random variable indicating the current node of the walker, $\mathbf{Y}$ the random variable indicating the node to which the walker will move in the next time step, and $\mathbf{T}$ the random variable indicating the target node where the walk will terminate (we assume that all nodes can be reached from all nodes in finite time). For all t, we denote the transition probabilities at $\mathbf{X} = i$ as:

$p^t_{ij} = Pr(\mathbf{Y} = j|\mathbf{X} = i,\mathbf{T} = t)$ where $\sum_j p^t_{ij} = 1$, and $p^t_{ij} = 0$ when there is no connection between nodes i and j. Finally, the walk ends when $i = t$, in which case $p^t_{ij} = 1$ for $j = t$ and 0 for all other j. Formally, the network dynamics for each separate target t form a Markov chain with state t as an absorbing state (see Methods). The set of transition probabilities for all t express the routing strategy that governs the dynamics of walkers (signals) navigating the network.

We specify transition probabilities at every node using a family of dynamical processes that combine local and global information about the network's topology. To this end, we define the dynamics of the system by tuning a global information bias using the following stochastic model:

$$P_\lambda(\boldsymbol{Y} = j|\boldsymbol{X} = i, \boldsymbol{T} = t) = \exp(-(\lambda(d_{ij} + g_{jt}) + d_{ij}))\frac{1}{Z^t_i} \quad (1)$$

where $Z^t_i = \sum_j \exp(-(\lambda(d_{ij} + g_{jt}) + d_{ij}))$ is a normalization factor. Transition probabilities are governed by two sources of information:

- a *local* source of information d_{ij} denoting the length of the edge connecting i and j ($d_{ij} \neq \infty$ if and only if a connection between i and j exists).
- a *global* source of information $d_{ij} + g_{jt}$, denoting the minimum distance from node i to target t though node j. This is the sum of the distance between node i and neighbor node j (d_{ij}), plus the distance from node j to the target node t through the shortest path (g_{jt}—note that this term has no dependence on i).

The parameter λ controls the extent to which transition probabilities are shaped by global information. Most importantly, λ gradually changes the dynamics on the network from an unbiased random walk towards a shortest-path routing strategy (see Fig 1):

- When λ = 0, a walker's motion is driven only by local information. Transition probabilities are simply given by $P_\lambda(\boldsymbol{Y} = j|\boldsymbol{X} = i, \boldsymbol{T} = t) = \exp(-d_{ij})\frac{1}{Z_i^t}$ and do not depend on the target node (nonetheless, the walk still terminates when it eventually reaches the target node t). In the case of brain networks, where edge-weights express connection strengths or node proximities in the interval (0,1) (this can always be enforced through a unique linear

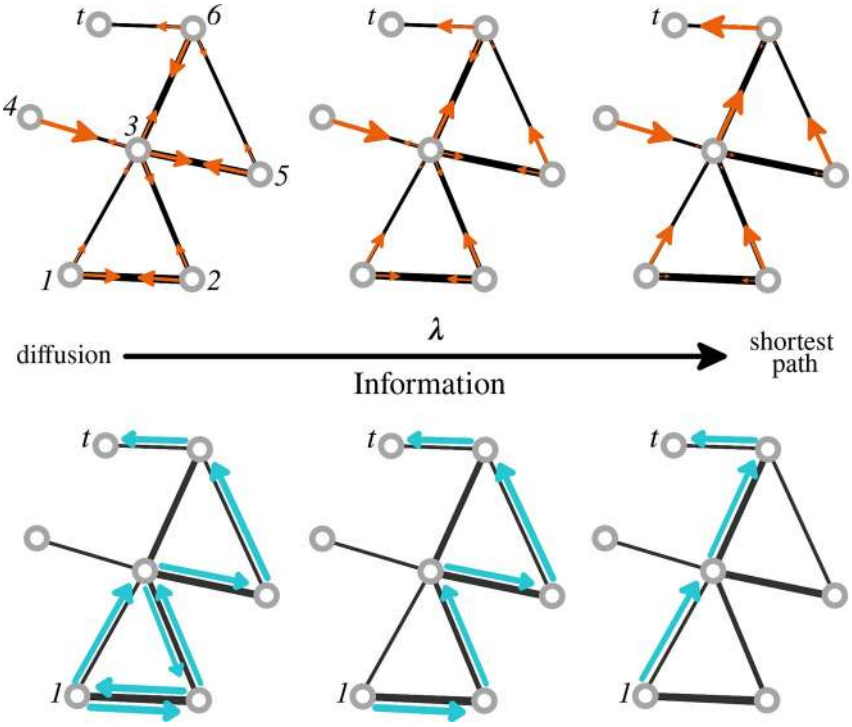

Fig 1. A spectrum of routing strategies. The parameter λ controls the extent to which routing strategies (transition probabilities) are reshaped by global information. Toy networks in the top row illustrate how transition probabilities, represented by orange arrows, are reshaped as the parameter λ increases. At each node, the orange arrows are proportional to the probability of a walker moving to a neighboring node via that edge. Blue arrows on the toy networks in the bottom row illustrate a possible walk followed by a random walker (signal) going from node *1* to node *t*, while operating according to the routing strategy represented by the orange arrows. When λ = 0, transition probabilities at each node are proportional to the strength of its connections. Random walkers operating under this routing strategy (the *reference navigation strategy*, P^{ref}) diffuse through the network until they eventually arrive at the target node. When $\lambda \to \infty$, transition probabilities at each node route walkers through the shortest path to the target node; a walker starting at node 1 will follow the shortest path to node t, as illustrated by the blue arrows. In the middle of the spectrum, walker's dynamics are influenced by global information but still driven partially by local topological properties. Notice that only transition probabilities vary with λ while the underlying network structure remains invariant.

https://doi.org/10.1371/journal.pcbi.1006833.g001

normalization function [32,33]; See Methods), we apply the proximity-to-distance function $d_{ij} = -\log(w_{ij})$ and map all edge-weights onto edge-distances. The resulting dynamics $P_0(\boldsymbol{Y} = j|\boldsymbol{X} = i, \boldsymbol{T} = t) = w_{ij}\frac{1}{s_i}$, where $s_i = \sum_j w_{ij}$ is the strength of node i, defines an unbiased random walk on the network where walkers favor transitions through edges with shorter connection distances (i.e. closer proximities). We refer to the unbiased random walk as the *reference navigation strategy*, P^{ref}, as it represents a null model of navigation that would naturally take place on the network if no bias is introduced.

- When $\lambda \to \infty$ global information governs the model and transition probabilities converge to $P^t_{ij} = 1$ if the edge $\{i, j\}$ lies on the (unique) shortest path between i and t (degenerate shortest paths, i.e. more than one shortest path from i to t, are less common in weighted networks, compared to unweighted networks, but see Methods for the case where degenerative shortest paths exist) and $p^t_{ij} = 0$ otherwise. Hence, statistics computed on such walks will correspond to a "shortest-path" routing strategy—in particular average walk length will be equal to shortest path length.

It is worth noting that the model acts on the routing strategies by changing the transition probabilities at each node, but we assume that the topology and weight structure of the network remain unchanged (see Fig 1). This procedure was formally introduced by Lambiotte et al [27], who showed that a biased random walk on a network A can be interpreted as an unbiased random walk on an appropriately defined flow graph A', where the weights of the connections of A' dictate the patterns of flow of a diffusion process at equilibrium.

The cost of reshaping the system's dynamics

We are interested in characterizing the *communication cost* of the dynamics generated by our model as we gradually increase λ, therefore increasing the global information bias on the dynamics. Here, we focus on two aspects of the cost associated with a communication process. First, we consider a *transmission cost*, which is the cost associated with messages being transmitted from one node to another. Second, we consider an *informational cost*, which is the cost associated with using global information to reshape the system's dynamics and thus route messages efficiently.

We consider a walker navigating the network and acting according to the routing strategies $P_\lambda(\mathbf{Y}|\ \mathbf{X},\mathbf{T})$. Let $c^{trans}_\lambda(i,t) = \sum_j P_\lambda(\mathbf{Y} = j|\ \mathbf{X} = i,\mathbf{T} = t)\ d_{ij}$ be the *immediate transmission cost* at node i for a walker going to node t with routing strategy $P_\lambda(\mathbf{Y}|\ \mathbf{X} = i,\mathbf{T} = t)$. The *immediate transmission cost* quantifies the cost associated with $\mathbf{X} = i$ partaking in the communication process by relaying the message to one of its neighbors, and in this setting it is equivalent to the expected distance that a walker at node i has to travel to move to a neighbor of i. Let $\mathrm{n}^t_\lambda(i,k)$ be the mean number of times node k is visited by a walker starting at a source node $\mathbf{X}_0 = i$ and acting according to a routing strategy $P_\lambda(\mathbf{Y}|\ \mathbf{X} = i,\mathbf{T} = t)$. We define the transmission cost of a walk starting at source node $\mathbf{X}_0 = i$ and terminating at the target node t as the sum of the *immediate transmission costs* accumulated at each visited node along a walk, that is $C^{trans}_\lambda(i,t) = \sum_k \mathrm{n}^t_\lambda(i,k)\ c^{trans}_\lambda(k,t)$. Thus, a walk's transmission cost is equivalent to the mean walk length between nodes i and t, under the routing strategy defined by λ. Noting that the transmission cost is not a symmetric measure, (i.e. $C^{trans}_\lambda(i,t)$ may not be the same as $C^{trans}_\lambda(t,i)$, except for when $\lambda \to \infty$), we can define the average transmission cost of a node acting as a source as $\overrightarrow{C}^{trans}_\lambda(i) = \frac{1}{N}\sum_t C^{trans}_\lambda(i,t)$, and the average transmission cost of a node acting as a target as $\overleftarrow{C}^{trans}_\lambda(t) = \frac{1}{N}\sum_i C^{trans}_\lambda(i,t)$. These measures quantify the *source and target closeness centrality* of

each node under a routing strategy: $\overrightarrow{C}_{\lambda}^{trans}(i)$ quantifies the average walk length from a node i to any other target node in the network, whereas $\overleftarrow{C}_{\lambda}^{trans}(t)$ quantifies the average walk length from any source node to the target node t.

To quantify the informational cost associated with routing messages to a target node t under the routing strategy $P_{\lambda}(\mathbf{Y}|\ \mathbf{X} = i,\mathbf{T} = t)$, we define $c_{\lambda}^{info}(i,t) = \mathrm{KL}(P_{\lambda}(\mathbf{Y}|\ \mathbf{X} = i,\mathbf{T} = t)||\ P^{ref}(\mathbf{Y}|\ \mathbf{X} = i,\mathbf{T} = t))$ as the *informational cost* at node $\mathbf{X} = i$, measuring the Kullback-Leibler divergence between the routing strategy $P_{\lambda}(\mathbf{Y}|i,t)$ and the null model or reference routing strategy $P^{ref}(\mathbf{Y}|i,t)$. The Kullback-Leibler divergence measures the additional bits of information required to manipulate the outgoing transition probabilities at a given node, and adopt a routing strategy that deviates from the reference routing strategy, $P^{ref}(\mathbf{Y}|i,t)$. Hence,the *informational cost* quantifies the effect of the global information bias by measuring the extent to which the biased dynamics $P_{\lambda}(\mathbf{Y}|i,t)$ deviate from $P^{ref}(\mathbf{Y}|i,t)$at node $\mathbf{X} = i$ [34].

Then, the informational cost of routing a message from a starting at node $\mathbf{X} = i$ to a target node t is the weighted average *informational cost* across all nodes in the network, weighted by the frequency with which each node is visited along the walk: $C_{\lambda}^{info}(i,t) = \sum_k \left(\frac{n_{\lambda}^{t}(i,k)}{\sum_r n_{\lambda}^{t}(i,r)} c_{\lambda}^{info}(k,t) \right)$. Finally, we can define the average informational cost of a node acting as a source as $\overrightarrow{C}_{\lambda}^{info}(i) = \frac{1}{N}\sum_t C_{\lambda}^{info}(i,t)$, and the average informational cost of a node acting as a target as $\overleftarrow{C}_{\lambda}^{info}(t) = \frac{1}{N}\sum_i C_{info}^{\lambda}(i,t)$.

It is important to note that, in order to model the system's dynamics and construct a matrix of transition probabilities $P_{\lambda}(\mathbf{Y}|\ \mathbf{X},\mathbf{T})$, the shortest path-length between all node pairs (i.e. the global information term $d_{ij} + g_{jt}$) is required, for any $\lambda > 0$, as an input parameter to the model. Once $P_{\lambda}(\mathbf{Y}|\ \mathbf{X},\mathbf{T})$ are defined by the model, the knowledge about the global topology becomes "fuzzy" or probabilistic andthe dynamics become autonomous; the walker trajectories on the network will evolve according to the dynamics dictated by $P_{\lambda}(\mathbf{Y}|\ \mathbf{X},\mathbf{T})$. There is no need for the neural elements to store the global information in a table, as any information about the global topology is "implicitly encoded" as a bias on the random walk, and the degree of such bias is precisely what we quantify with the informational cost measure.

In the following sections we will study the communication costs of routing strategies generated by our stochastic model applied to the structural brain connectivity matrices of two cohorts of healthy subjects. In the main text, we focus on 173 unrelated subjects from the Human Connectome Project (HCP) dataset [35,36]. The Supplementary S1–S5 Figs show results from the replication dataset (LAU), composed of 40 healthy subjects (see Methods). We first analyze cost measures at the global, nodal, and pairwise level, measured and averaged across all subjects (within each cohort). Lastly, we examine individual subject differences with respect to the proposed cost measures. We emphasize that our aim is not to identify a routing strategy for brain communication, but instead, to expose a spectrum of communication dynamics that unifies the classical shortest-paths routing vs. diffusion dichotomy [12,37].

Brain networks are more efficient within an intermediate region of the communication spectrum

By construction, the transmission and informational cost have a competing relationship (or trade-off) such that as we increase λ in the stochastic model, the mean walk lengths (C_{λ}^{trans}) of messages acting according to P_{λ} become shorter while the bias effect due to global information (C_{λ}^{info}) increases. This trade-off is shown in Fig 2A where averages of C_{λ}^{trans} and C_{λ}^{info} across all $\{i,t\}$ pairs are plotted as a function of λ. It can be seen that C_{λ}^{trans}, measuring the average walk

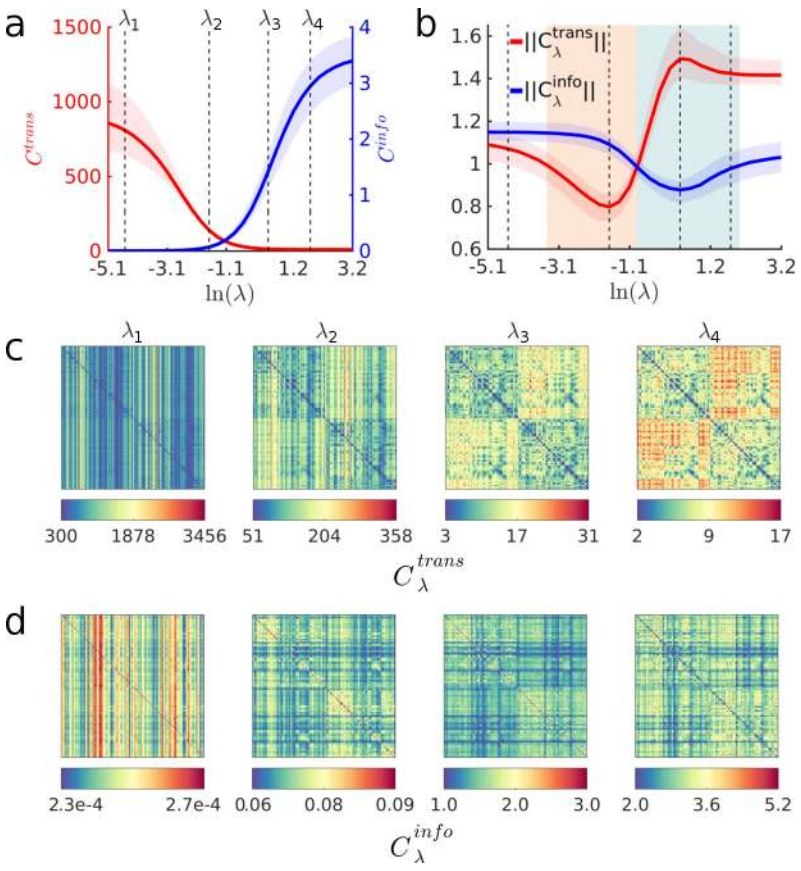

Fig 2. A spectrum of communication processes. (a) Averages of C_λ^{trans} (red) and C_λ^{info} (blue) across all node pairs, as a function of λ. Solid red and blue lines correspond to the median across all subjects, whereas the shaded red and blue regions denote the 95th percentile. (b) Averages of $||C_\lambda^{trans}||$ (red) and $||C_\lambda^{info}||$ (blue) across all node pairs. These curves are computed by normalizing C_λ^{trans} and C_λ^{info} with respect to the same cost measures computed on ensembles of 500 randomized networks (per subject). Shaded red and blue areas indicate sections of the curves $||C_\lambda^{trans}||$ and $||C_\lambda^{info}||$ that are smaller than 1, respectively, indicating the regions in the spectrum where the communication cost of empirical networks (i.e. networks that are derived from empirical data) is smaller than the cost computed on the randomized ensembles. The dashed vertical lines are placed at the minimum and maximum of $||C_\lambda^{trans}||$ (λ_2 and λ_3, respectively), and at two points near the extremes of the spectrum (λ_1 and λ_4). (c) pairwise values of $C_\lambda^{trans}(i,t)$ for all node pairs. (d) pairwise values of $C_\lambda^{info}(i,t)$ for all node pairs. In all panels, $\lambda_1 = e^{-4.49}$, $\lambda_2 = e^{-1.64}$, $\lambda_3 = e^{0.37}$ and $\lambda_4 = e^{1.79}$.

https://doi.org/10.1371/journal.pcbi.1006833.g002

length, approaches a shortest path-length regime at around λ = 1 (ln(λ) = 0 in Fig 2), suggesting that in this regime messages can be efficiently routed at a low informational cost.

Next, we consider an ensemble of random networks and compare average transmission and informational costs incurred in empirical brain networks and in randomized ensembles of networks. All randomized networks preserve node degree, node strength (evaluated with respect to the proximity edge-weights), and the network's weight distribution (see Methods). We generate routing strategies P_λ for all randomized networks and normalize the cost measures C_λ^{trans} and C_λ^{info} of each subject's empirical brain network with respect to the average cost measures computed across the corresponding randomized counterparts. Fig 2B shows normalized cost measures $||C_\lambda^{trans}|| = C_\lambda^{trans}(emp)/C_\lambda^{trans}(rand)$ (red line) and $||C_\lambda^{info}|| = C_\lambda^{info}(emp)/C_\lambda^{info}(rand)$ (blue line) as a function of λ. In accordance with prior work (37–39), we find that average walk lengths are shorter for random networks (i.e. $||C_\lambda^{trans}|| > 1$) at the extremes of the spectrum, representing the unbiased random walk (P^{ref}) and shortest path regimes. Interestingly,

our analysis reveals an interval of λ values (shaded region in Fig 2B) for which empirical networks exhibit shorter walk-lengths compared to the randomized counterparts (i.e. $\|C_\lambda^{trans}\| < 1$). Moreover, the informational cost behaves similarly, although the regions $\|C_\lambda^{info}\| < 1$ and $\|C_\lambda^{trans}\| < 1$ barely overlap. Overall, these results show that the randomized counterparts of empirical brain networks are more efficient only at the extremes of the communication spectrum.

Fig 2C and 2D show pairwise C_λ^{trans} and C_λ^{info} (median across subjects) computed for routing strategies generated with $\lambda_1 = e^{-4.49}$, $\lambda_2 = e^{-1.64}$, $\lambda_3 = e^{0.37}$ and $\lambda_4 = e^{1.79}$ (see dashed vertical lines in Fig 2A and 2B). These values of λ correspond to two points located near the extremes of the communication spectrum, and two points located at the minimum and maximum of the curve $\|C_\lambda^{trans}\|$, where the empirical networks are most and least efficient compared to their randomized counterparts. As evidenced by the column-like patterns in the matrices corresponding to λ_1 and λ_2, the dynamics of messages navigating the network are strongly determined by the local connectivity of the target node when the global information bias is small. As the bias increases and routing strategies depart from the reference strategy P^{ref}, the dynamics of messages are less dependent on the target node only. Finally, as walk-lengths converge towards shortest-path, the transmission cost becomes symmetric, i.e., $C_\lambda^{trans}(i,t) = C_\lambda^{trans}(t,i)$.

Source vs. target communication cost

We now analyze cost measures at the nodal level. Fig 3A and 3B show scatter plots of the average source and target transmission costs ($\overrightarrow{C}_\lambda^{trans}$ and $\overleftarrow{C}_\lambda^{trans}$, respectively), and the average source and target informational costs ($\overrightarrow{C}_\lambda^{info}$ and $\overleftarrow{C}_\lambda^{info}$, respectively) associated to all nodes (median across all subjects) for the same values of λ highlighted in Fig 2. Nodes are colored according to their membership in functional intrinsic connectivity networks (ICNs; see Methods), highlighting a tendency of some ICNs to contain an overabundance of costly sources and/or targets, while other ICNs' cost varies as a function of λ. Interestingly, nodes belonging to the unimodal networks, namely the visual (VIS, colored red) and somatomotor (SM, colored green) networks, exhibit less variability across cost measures. Nodes belonging to the somatomotor network tend to exhibit a high $\overrightarrow{C}_\lambda^{trans}$ and low $\overleftarrow{C}_\lambda^{trans}$ for $\lambda < e^{0.37}$, while they also exhibit a consistent low $\overrightarrow{C}_\lambda^{info}$; nodes belonging to the visual network exhibit high $\overrightarrow{C}_\lambda^{info}$ and $\overleftarrow{C}_\lambda^{info}$ for $\lambda > e^{-4.49}$, while $\overrightarrow{C}_\lambda^{trans}$ and $\overleftarrow{C}_\lambda^{trans}$ vary as a function of λ. We also note that the dorsal attention regions (DA, colored purple) consistently exhibit low $\overrightarrow{C}_\lambda^{trans}$ and $\overleftarrow{C}_\lambda^{trans}$ for $\lambda > e^{-4.49}$.

In order to assess to what extent high or low nodal costs are driven by the network's overall topology, as opposed to nodal degree or strength distribution, we standardize nodal costs with respect to the corresponding nodal cost distributions measured on the randomized network ensembles. Significantly high or low standardized nodal cost measures are indicative of global connectivity patterns that are encountered only in empirical brain networks. Supplementary S6 and S7 Figs show thresholded z-scores ($\alpha = 0.01$) for all nodal cost measures as a function of lambda. As expected, near the extremes of the spectrum ($\lambda = 0$ and $\lambda > 1$), most nodes exhibit significantly higher costs, compared to the randomized networks, however, significantly low cost regions are found in the middle of the spectrum. Prominent low $\overrightarrow{C}_\lambda^{info}$ regions include the right and left hemisphere frontal, precentral, paracentral and postcentral regions; low $\overleftarrow{C}_\lambda^{info}$ regions include the right and left posterior cingulate, the supramarginal gyrus, the superior parietal cortex, the precuneus, and the inferior parietal cortex. Prominent low $\overrightarrow{C}_\lambda^{trans}$ regions are mainly located in the frontal cortex (frontal pole, medial orbital frontal and rostral

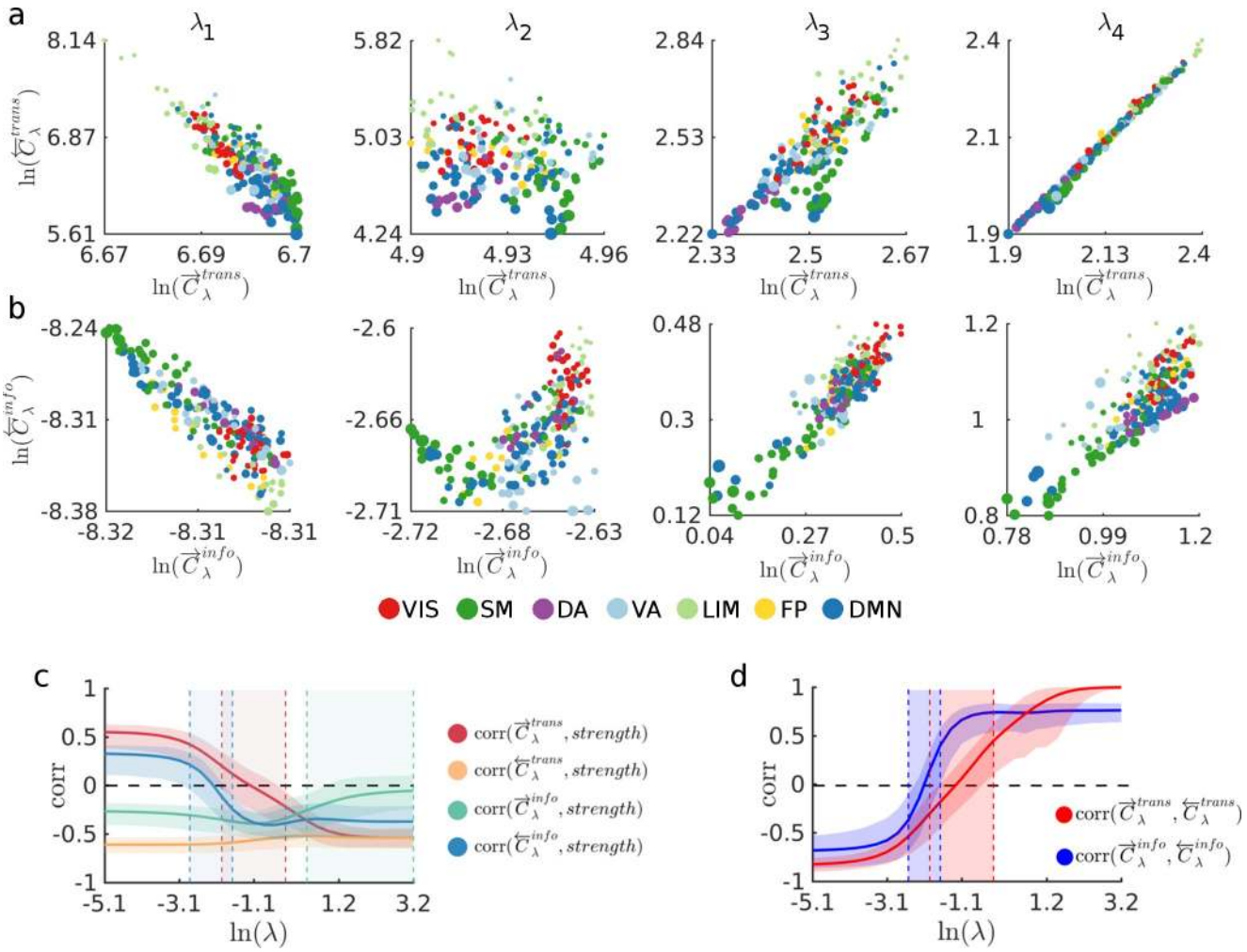

Fig 3. Nodal average transmission costs for four increasingly biased routing strategies. (a) Scatter plots show the transmission cost associated to each node when it acts as source ($\overrightarrow{C}_{\lambda}^{trans}$) and target ($\overleftarrow{C}_{\lambda}^{trans}$) during communication processes taking place under routing strategies generated with the values λ_1, λ_2, λ_3 and λ_4. (b) Scatter plots show the informational cost associated to each node when it acts as source ($\overrightarrow{C}_{\lambda}^{info}$) and target ($\overleftarrow{C}_{\lambda}^{info}$) during communication processes taking place under routing strategies generated with the values λ_1, λ_2, λ_3 and λ_4. Markers in the scatter plots in (a) and (b), representing each node, are colored according to the node's membership in the 7 intrinsic connectivity networks (ICN) defined by Yeo et al. (2011) [71]: Visual (VIS), Somatomotor (SM), Dorsal Attention (DA), Ventral Attention (VA), Limbic (LIM), Frontal Parietal (FP), and Default Mode Network (DMN). The size of the markers is proportional to node's strength. (c) Correlations between node strength and $\overrightarrow{C}_{\lambda}^{trans}$ (red), $\overleftarrow{C}_{\lambda}^{trans}$ (orange), $\overrightarrow{C}_{\lambda}^{info}$ (green) and $\overleftarrow{C}_{\lambda}^{info}$ (blue) as a function of λ. Solid lines show median correlation across all subjects, shaded areas surrounding the lines show 95th percentile. Shaded colored areas between the vertical dashed lines indicate regions where the correlations were not significant ($p > 0.001$). (d) Correlation between $\overrightarrow{C}_{\lambda}^{trans}$ and $\overleftarrow{C}_{\lambda}^{trans}$ (red), and $\overrightarrow{C}_{\lambda}^{info}$ and $\overleftarrow{C}_{\lambda}^{info}$ (blue), as a function of λ. Solid lines show medians across all subjects and shaded areas surrounding solid lines show the 95th percentile. Shaded areas between the vertical dashed lines indicate areas where correlation values were not significant ($p > 0.001$). In all panels, $\lambda_1 = e^{-4.49}$, $\lambda_2 = e^{-1.64}$, $\lambda_3 = e^{0.37}$ and $\lambda_4 = e^{1.79}$.

https://doi.org/10.1371/journal.pcbi.1006833.g003

middle frontal regions), right and left superior parietal regions, the right and left precuneus, and the left cuneus. Interestingly, no significantly low $\overleftarrow{C}_{\lambda}^{trans}$ regions were identified, suggesting that randomized topology favors all regions as routing targets, but not as routing sources.

Our analyses also reveal a varying relationship (as a function of λ) between the nodal cost measures and node strength (see Fig 3C). At the extremes of the spectrum, transmission cost is strongly driven by node strength. When λ = 0, the correlation between node strength and $\overrightarrow{C}_{\lambda}^{trans}$ and $\overleftarrow{C}_{\lambda}^{trans}$ is $r = 0.55$ and $r = -0.61$, respectively ($p < 0.001$), indicating that high strength

nodes (hubs) are costly sources but low cost targets with respect to transmission cost. In other words, when the global information bias is low (or zero), messages can be routed at a low transmission cost from any brain region to a hub; conversely, routing a message from a hub to any brain region incurs a high transmission cost. At the other end of the spectrum (i.e. for large values of λ), hub nodes are low cost sources and targets with respect to transmission cost ($r = -0.53$, $p<0.001$; note that the orange and red lines in Fig 3C converge). However, in the middle of the spectrum, the average correlation between node strength and $\overrightarrow{C}_{\lambda}^{trans}$ is close to zero, whereas the correlation between node strength and $\overleftarrow{C}_{\lambda}^{trans}$ remains significant ($r \approx -0.5$, $p<0.001$) throughout the entire spectrum. This varying relationship between node strength and cost measures as a function of λ highlights a distinction between the dynamical measures proposed here, and static centrality measures that rely only on the network's structure. Static measures such as betweenness centrality, page rank [38] and communicability [39], are strongly driven by nodal degree or strength (See Supplementary S1 Text showing a comparison between C_{λ}^{trans} and a set of static centrality measures), but are blind to the patterns of flow imposed by the network structure and the dynamics of the system.

The relationship between source and target costs also varies as a function of λ (see Fig 3D). For low values of λ, both $\overrightarrow{C}_{\lambda}^{trans}$ and $\overleftarrow{C}_{\lambda}^{trans}$, and $\overrightarrow{C}_{\lambda}^{info}$ and $\overleftarrow{C}_{\lambda}^{info}$ are negatively correlated. In other words, nodes that are costly sources are efficient targets, and nodes that are costly targets are efficient sources. However, the correlations undergo a sign flip as λ increases and $\overrightarrow{C}_{\lambda}^{trans}$ and $\overleftarrow{C}_{\lambda}^{trans}$, and $\overrightarrow{C}_{\lambda}^{info}$ and $\overleftarrow{C}_{\lambda}^{info}$ become positively correlated. Note that the correlation between $\overrightarrow{C}_{\lambda}^{trans}$ and $\overleftarrow{C}_{\lambda}^{trans}$ converges to 1 as these two measures are identical at the shortest-path extreme (the symmetry between $\overrightarrow{C}_{\lambda}^{trans}$ and $\overleftarrow{C}_{\lambda}^{trans}$ at the shortest path extreme will hold for any undirected network).

A node's propensity to be a costly transmission/informational source or target is projected onto the cortical surface in Fig 4, where we show the difference between a node's source and target costs for $\lambda_1 = e^{-4.49}$, $\lambda_2 = e^{-1.64}$, $\lambda_3 = e^{0.37}$ and $\lambda_4 = e^{1.79}$ (same values highlighted in Fig 2

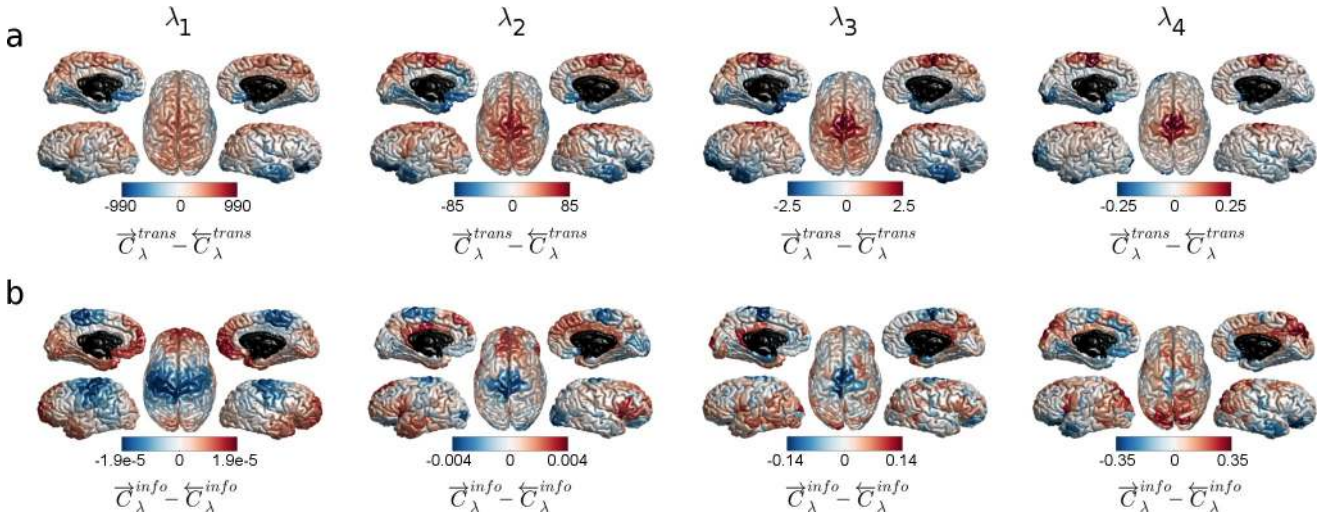

Fig 4. A brain region's propensity to be a costly source or target. Cortical surfaces show the difference between a node's source and target transmission costs. (a) $\overrightarrow{C}_{\lambda}^{trans} - \overleftarrow{C}_{\lambda}^{trans}$ for routing strategies generated with the values λ_1, λ_2, λ_3 and λ_4. (b) $\overrightarrow{C}_{\lambda}^{info} - \overleftarrow{C}_{\lambda}^{info}$ for routing strategies generated with the values λ_1, λ_2, λ_3 and λ_4. Red colored areas on the cortical surfaces correspond to nodes whose source transmission/informational cost is higher than their target transmission/informational cost. Blue colored areas correspond to nodes whose target transmission/informational cost is higher than their source transmission/informational cost. In all panels, $\lambda_1 = e^{-4.49}$, $\lambda_2 = e^{-1.64}$, $\lambda_3 = e^{0.37}$ and $\lambda_4 = e^{1.79}$.

https://doi.org/10.1371/journal.pcbi.1006833.g004

and Fig 3). Cortical regions that are costly sources (compared to the cost of being a target) are colored red whereas regions that are costly targets (compared to the cost of being a source) are colored blue. This analysis reveals that dorsal portions of the precentral and postcentral gyri are increasingly costlier sources in terms of transmission cost, whereas frontal regions of the temporal lobes and inferior frontal areas are increasingly costlier targets, as λ increases. In terms of informational cost, we see the opposite relationship in the same anatomical regions, but the informational cost differences decrease as λ increases.

Routing strategies for privileged nodes

In this section we will explore a different scenario where, in the interest of economizing on informational cost, we allow only a subset of *privileged nodes* to be affected by the global information bias. We consider increasingly larger size sets of r privileged nodes that are able to reshape their routing strategies according to the influence of global information. Privileged nodes are selected according to different node centrality rankings. Given a centrality-based ranking of nodes, we generate routing strategies for the r-highest ranked (privileged) nodes according to the stochastic model, where λ is an attribute that only applies to the set of privileged nodes; all *non- privileged nodes'* routing strategies remain unbiased and are equal to $P^{ref}(\mathbf{X})$. The left and middle panel of Fig 5 show network average values of C_λ^{trans} and C_λ^{info} (median across all subjects) as a function of λ for varying fractions of *privileged nodes* that are selected according to various centrality-based rankings. The black dotted lines show C_λ^{trans} and C_λ^{info}, respectively, for the case in which all nodes' routing strategies are biased.

This approach reveals three interesting properties about the routing capacity of the brain. First, the composition of the set of privileged nodes matters, as evidenced by the differences in C_λ^{trans} and C_λ^{info} that are obtained as the set size and composition is varied. Second, for a fixed number of privileged nodes, the more the system economizes on informational cost, the more it expends on transmission cost. For example, routing strategies where we select privileged nodes according to betweenness centrality ranking yield smaller C_λ^{trans} and larger C_λ^{info} throughout the entire spectrum, compared to other centrality-based privileged node selections. Conversely, routing strategies where we select privileged nodes according to a random walk centrality ranking are the most costly in terms of C_λ^{trans}, but least costly in terms of C_λ^{info}. Third, a small number of strategically selected privileged nodes can achieve a C_λ^{trans} that approximates the C_λ^{trans} achieved when all nodes are subject to the global information bias. To show this, we compute the stretch of a walk [25] defined as the absolute difference between optimally shortest path lengths obtained when all nodes' dynamics are biased by global information, and shortest walk length obtained when only privileged node's dynamics are biased by global information. Node stretch distributions (medians across all subjects) are shown in the right-side panel of Fig 5. We note that when the top 25% betweenness centrality nodes are selected as privileged nodes, the average stretch is only 4.2, in contrast to a stretch of 12.7 obtained when the top 25% random walk closeness centrality nodes are selected. Overall, these results indicate that efficient routing patterns can emerge even when less than half of the nodes are capable of routing information.

A communication cost trade-off within subjects

Our approach allows us to study the variability of communication cost measures across subjects. We first examine whether subjects who exhibit higher values of C_λ^{trans} at $\lambda = 0$ (that is, longer walk lengths for the unbiased random walk) will maintain a high C_λ^{trans} throughout the entire spectrum. Fig 6A shows correlations between all subject's C_λ^{trans} across all values of λ.

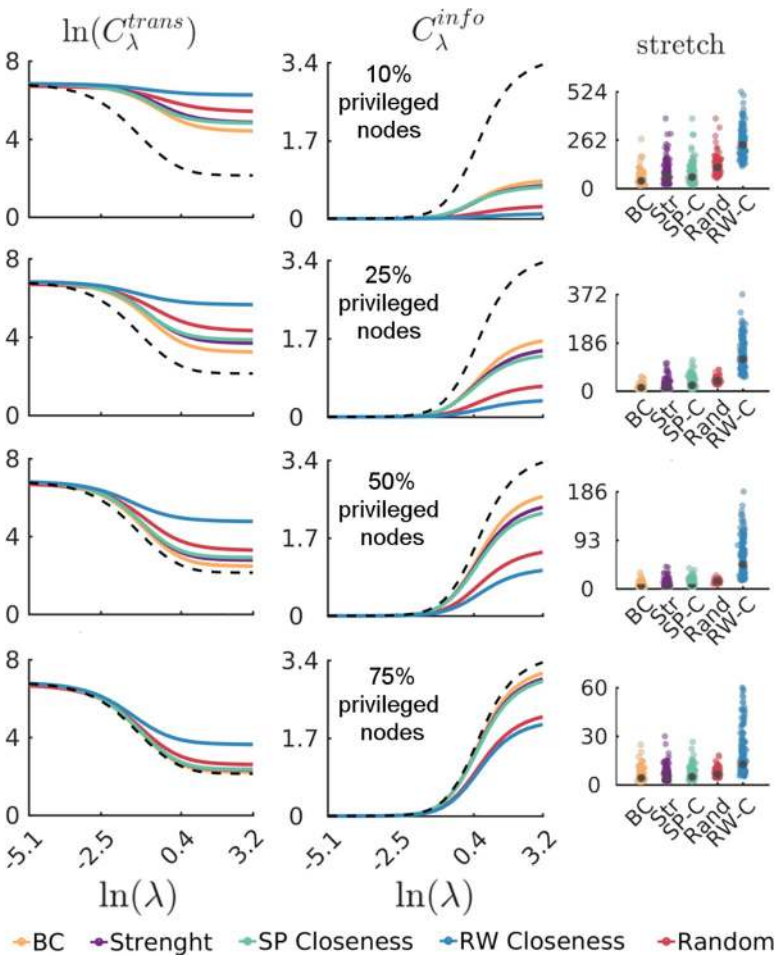

Fig 5. Routing strategies for privileged nodes. Network average values of C_λ^{trans} (left panel) and C_λ^{info} (middle panel) as a function of λ (node medians across all subjects) for 22, 55, 110, and 165 *privileged nodes* (corresponding to 10%, 25%, 50% and 75% of the network's nodes) that are selected according to betweenness centrality ranking (yellow line), strength ranking (purple line), shortest-path-based closeness centrality (green line), and random-walk-based closeness centrality (blue line). For comparison purposes, we also show cost measures for randomly sampled nodes (red line represents average across 500 samples). The dotted lines show C_λ^{trans} and C_λ^{info}, respectively, for the case in which all nodes' routing strategies are biased (i.e. 100% privileged nodes). Right panel shows node stretch distributions for the different sets of privileged nodes and centrality rankings. Black markers indicate the median of the distributions.

https://doi.org/10.1371/journal.pcbi.1006833.g005

These correlations show that subjects who exhibit higher values of C_λ^{trans} at $\lambda < e^{-3.1}$ are also subjects with the highest C_λ^{trans} at $\lambda > 1$, but the relationship is inverted in the middle of the spectrum.

Finally, we investigate if there are differences in how individual subject's brain networks take advantage of the global information bias. We address this question by measuring the area under each subject's C_λ^{trans} curve and C_λ^{info} curve. Moreover, since we are interested in capturing the rate of decay and growth of subject's C_λ^{trans} and C_λ^{info} curves, we first normalize each subject's C_λ^{trans} curve with respect to C_λ^{trans} at $\lambda = 0$ (that is, the average length of unbiased random walks), and we normalize each subject's C_λ^{info} curve with respect to C_λ^{info} at $\lambda = e^{3.2}$ (that is, the max value of C_λ^{info}). The normalized C_λ^{trans} and C_λ^{info} curves of 8 subjects are shown in Fig 6B, illustrating curves that decay/grow faster with λ, which we can capture by measuring the area under the curve. Fig 6C shows a scatter plot of the areas under the normalized C_λ^{trans} and C_λ^{info} curves

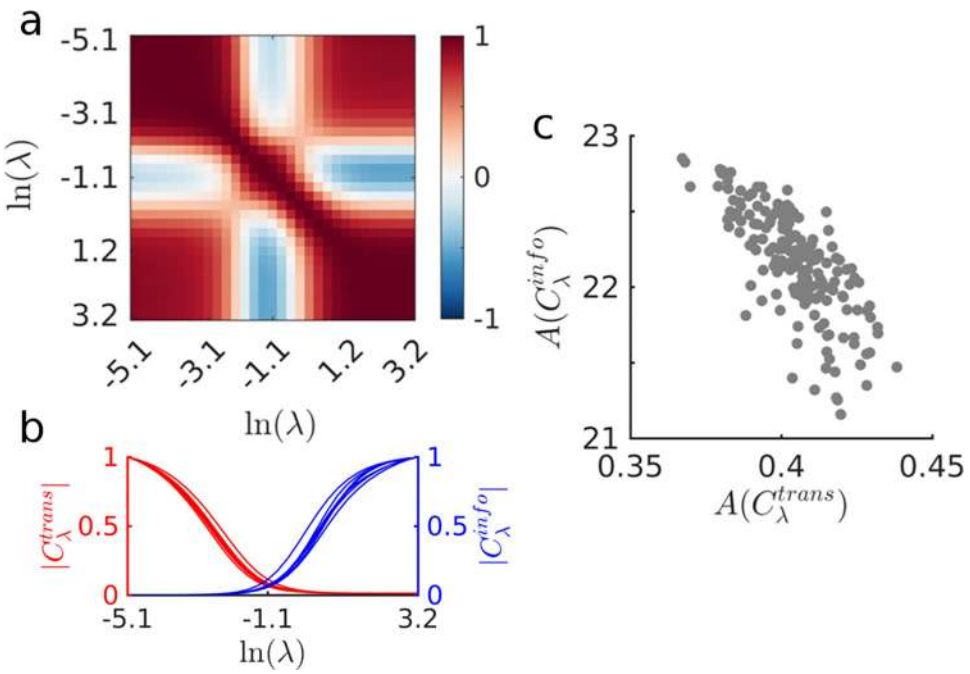

Fig 6. Communication cost trade-off within subjects. (a) Correlations between all subject's C_λ^{trans} across all values of λ. Positive correlations are colored in red, negative correlations are colored in blue. (b) Eight subject's C_λ^{trans} and C_λ^{info} curves after normalization with respect to the max(C_λ^{trans}) and max(C_λ^{info}), respectively. Notice how some subject's C_λ^{trans} curves decay faster than others, and how some subject's C_λ^{info} curves grow faster than others. (c) Scatter plot of the computed areas under the normalized C_λ^{trans} and C_λ^{info} curves, sowing a trade-off between the decay of C_λ^{trans} and the growth of C_λ^{info} (the correlation between A(C_λ^{trans}) and A(C_λ^{info}) is $r = -0.74$, $p < 0.001$).

https://doi.org/10.1371/journal.pcbi.1006833.g006

of all subjects, exhibiting a strong negative correlation between the normalized areas under C_λ^{trans} and C_λ^{info} ($r = -0.74$, $p<0.001$). This strong relationship indicates that there is a trade-off between a brain network's ability to take advantage of global information to route messages in a fast manner, and the amount of informational cost required to achieve optimally fast routing. How this trade-off is negotiated varies across individual subjects.

Discussion

The efficiency of communication in real world networks is not only determined by the speed with which messages are relayed, but the informational cost associated with selecting efficient routes is equally important. Here we introduce a stochastic model that generates routing strategies on a network by controlling the effect of global information over the actions of random walkers. We characterize the trade-offs between the cost of reshaping the system's dynamics (C_λ^{info}) and the cost of relaying messages through the network (C_λ^{trans}), and characterize these costs at a global, nodal and subject-wise level. Our results show that biased random walk dynamics can rapidly approach a shortest-path communication regime when afforded gradual small increases in the bias on global information. The concept of communication dynamics has become increasingly important in the context of brain networks [40,41]. Here, we address some of the assumptions behind two widely used brain communication models, namely routing and diffusion models. On the one side, communication that takes place through shortest paths assumes that neural elements are able to identify the optimal path and route a signal/message through such path; however, the mechanisms by which signals are routed and the

informational cost associated with routing them are rarely discussed. On the other side, communication that takes place through (unbiased) random walks assumes that signals are able to "bounce between nodes" for long periods of time. Yet, such a scheme raises issues about signal integrity and strength as well as metabolic cost. Our framework unifies these two extreme communication strategies under a family of communication models that can be characterized by the extent to which global information about the network topology biases the dynamics that shape the patterns of flow within the network.

Under the framework presented here, communication cost is not measured as a structural property of the network [17,24,37]. While wiring cost affects brain communication by means of being an important driver of brain geometry and network topology [1,17,15], it should be noted that wiring cost is a static property of the network (within relatively short time-scales) that is invariant under any communication process taking place on the network. In contrast, our framework approaches communication cost by considering two different cost components that are measured from the modeled dynamics of neural signals traversing the network under a specific routing strategy. First, we consider the transmission cost which we interpret as a proxy for the metabolic cost of transmitting neural signals from one neural node to another. It has been estimated that about 50% of the brain's energy is used to drive signals across axons and synapses [1], suggesting that energy consumption is a strong incentive to minimize the length of communication pathways in neural systems. Second, we consider the cost of reshaping the patterns of information flow (informational cost) that allow a signal to be efficiently routed towards a specific brain region. We conceptualize this cost as associated with modulatory processes that take place at the mesoscale or microscale, where signal traffic may be regulated as two neuronal population's firing rates change in order to synchronize and thus communicate [42], or as a process that emerges on top of the collective oscillatory dynamics of neural elements [43]. As our work is focused on macro-scale brain networks, it is important to note that we cannot claim that the signals we are modeling represent individual action potentials traveling along neuronal axons. Instead, we conceptualize neural signals as emerging from the coordinated activity of large populations of neuronal circuits and sub-systems. Under this higher order perspective, the signaling dynamics that we model represents the flow of information through the network's connections.

Our results contrast with well-established notions about the efficiency of random topologies [44,45], as we demonstrate that the randomized counterparts of empirical brain networks are only more efficient at the extremes of the communication spectrum. Interestingly, we find that within the regime where empirical networks are most efficient with respect to the randomized models, the frontal cortex has an overabundance of efficient source nodes, both in terms of information and transmission cost; conversely, the posterior and parietal regions of the cortex exhibit an overabundance of efficient target nodes in terms of information cost. We note that this behavior is only found in a limited regime that does not include the extremes of the communication spectrum. The implications of these findings are twofold. On the one hand, they demonstrate that cost-efficiency measures are relative to the communication process under consideration, and on the other hand, they raise questions regarding the use of appropriate null models as benchmarks to normalize graph-theoretic measures [12,46], as we have shown here that the randomized topology is not always more efficient than empirical networks.

Fundamentally, the cost measures that we consider here intrinsically capture the informational cost associated with traversing high-degree and high-strength nodes, that is, those comprising the brain's rich club. Indeed, it has been proposed that rich-club nodes facilitate integration of information within the network at the expense of a high wiring cost [24]; nonetheless, hubs are only advantageous for communication if signals can be routed through them, which implies high informational cost [47]. Here we show that at the low-information end of

the spectrum hub nodes are low cost targets but are high cost sources. It is only when we increase the global information bias that hubs become low cost sources and targets, but at the expense of an overall higher informational cost. Interestingly, a strong relationship between node degree, and the directionality with which signals are preferentially transferred through a network has been found in analytical, computational and empirical studies [48, 49], where it has been noted that high degree nodes' oscillatory activity lags in phase whereas low degree nodes' activity leads. These findings match the routing patterns that we find here but only at the low information-end of the spectrum, where hub nodes are efficient directional targets, while low degree nodes are efficient sources [49].

Our findings regarding the selection of privileged nodes that have access to global information show that some nodes are poised to take advantage of global information more efficiently than others; in brain networks, efficient routing patterns can be achieved by allowing as few as 25% of the highest betweenness or strength centrality nodes to reshape their routing strategies according to a bias on global information. These results offer a new perspective on the role of highly central nodes in facilitating the co-existence of functional integration and segregation between and within neural sub-systems: densely connected clusters of nodes (network communities) tend to "trap" random walkers [50] which promotes segregation, however a few well-connected privileged nodes that are specialized to direct the exchange of information between clusters can promote efficient integration of information. Hence, the *privileged nodes* framework presented here may provide some insight about the underlying communication processes allowing the exchange of information between modular sub-systems [51,52]. Finally, our study of individual differences not only expose an interesting trade-off between transmission and informational cost across subjects, but show that the measures are sensitive to individual differences. This is a promising avenue for future studies focusing on communication processes differences across clinical populations and human lifespan [53].

Several properties inherent in this framework have important implications for the future study of communication processes in brain networks. First, the routing patterns presented here are derived from a dynamical point of view, and not from a purely topological analysis of the system, allowing us to make use of well-established theoretical results about linear processes and biased random walks [21,26–31]. Second, discounting the extreme case of shortest path walks, the routing patterns generated by the model take place through multiple paths, promoting robustness to structural failures, and a higher tolerance to abundant signal traffic. Third, while we do not formally define a measure of communication efficiency in this study, it is worth noting that a natural derivation from the transmission cost measure results from its reciprocal (or inverse), thus extending and generalizing the global (or routing) efficiency [44] and diffusion efficiency [12,37] measures for shortest path and diffusion-based communication, respectively. Fourth, routing strategies at each node are dynamic, opening up the door to potential directions of further investigation focusing on the impact that functional demands and the availability of metabolic resources may have on the repertoire of routing patterns in brain networks. Finally, building on the concept of dynamic routing patterns, the notion of dynamic measures of centrality emerge naturally as a means to quantify the varying importance of nodes and edges under different underlying dynamics [27,31]. Here we have proposed the nodal cost measures $\overrightarrow{C}_{\lambda}^{trans}$, $\overleftarrow{C}_{\lambda}^{trans}$, $\overrightarrow{C}_{\lambda}^{info}$ and $\overleftarrow{C}_{\lambda}^{info}$ as dynamic source and target closeness centrality measures, but we note that additional centrality measures can be evaluated, such as the number of times that nodes are visited during a biased random walk (this centrality measure would converge to the betweenness centrality and random walk centrality at the extremes of the spectrum).

It is worth noting that the model we present here is only one way to formularize the spectrum between shortest paths and (unbiased) random-walk communication (see for example [54, 55]); different formulations of the spectrum may generate different families of communication models, which presume different assumptions about the cost of communication processes. For instance, our spectrum excludes communicability [39], a communication processes that takes into consideration all possible walks between a pair of brain regions. Like diffusion, communicability admits sub-optimal and parallel signal traffic, but unlike diffusion, communicability is blind to the patterns of flow imposed by the local properties of the network, and therefore, it presupposes some degree of knowledge about the global topology of the network in order to ensure that all walks of length k are equally likely to be used by signal traffic. Therefore, the informational cost measure that we propose here would not be appropriate to capture the informational cost of communicability.

Another subtle but important consideration is the question of how is global information made available to the system. The model we propose takes as an input parameter the global information about the network topology in the form of a pairwise shortest path distance. Therefore, the model does require full knowledge about the network topology. However, this does not imply that elements of the system have access to such information as this is a model of the dynamics, not a model for the underlying mechanisms that may generate the dynamics. It is still an open question how the system gains information about the global topology of the network, and what mechanisms dictate what connections are used to transmit neuronal signals. Biological systems are the product of evolution, adaptation, development and learning; one possibility is that, through these processes which continuously act to improve the system's performance, neural systems have gained information about their topology through feedback, resulting in an incremental update of the system's dynamics.

Some limitations are worth mentioning. First, for this study, our application of the stochastic model is limited by restricting λ to be a global attribute for all nodes, or for a set of privileged nodes; nonetheless, it is feasible (although computationally expensive) and perhaps more realistic to define λ as a continuously varying nodal property, $\lambda(i)$. Second, the stochastic model considers a scenario where communication between all nodes and a given target is equally salient. In systems such as the brain, where different sub-systems are associated with specific cognitive tasks, it is unlikely that all node pairs require the ability to efficiently exchange information with all other nodes. In this sense, the cost measures computed here may serve as an upper bound for the actual communication cost, however, it is important to keep in mind that our model does not consider issues of congestion that can arise as the traffic capacity of the network is exceeded [54,56].Third, linear dynamics may not be appropriate for systems that exhibit highly complex non-linear dynamics. Indeed, the brain is highly complex, topologically and dynamically. Yet, its complexity allows us to study it at different scales [57]. While it is clear that both structure and dynamics must be considered simultaneously to achieve a more comprehensive description of the system, it is still unclear how communication dynamics manifest at the various scales at which we are able to capture brain structure and dynamics. As pointed out in comparative analysis performed by Messe et al. [58], complex models of brain activity can effectively be reduced to simpler (linear) processes that are easier to dissect and understand. Hence, there is no evidence to discard linear dynamics as good approximation of the routing patterns taking place on large-scale brain networks. An interesting avenue to pursue is the exploration of higher-order models of flow, where transition probabilities are conditioned by past visited nodes. Finally, a goal for future work is the design of novel experimental strategies that can connect our current understanding of brain network topology and communication dynamics, illuminating the empirical problem of how brain networks integrate and process information in a manner that is adaptive, dynamic, flexible, and

cost efficient. Taken together, our work establishes a theoretical framework to study the efficiency of a broad range of communication processes on complex networks. While we have focused on a particular class of biased random walks where biases depend on the topological distance to target nodes, we note that biases may also depend on other aspects of the global topology or the embedding of a network in physical space [14,29]. Overall, this framework can be used to study any real world network that employs communication or navigation processes in its operation. It may be used, for instance, to infer pathways through which information is preferentially transferred, or, when such pathways are known, to infer the search and navigation strategies that allow accessing these pathways. In the context of brain networks, this theoretical framework may prove useful to identify efficient communication strategies that balance different aspects of the cost associated with neural communication.

Materials and methods

Ethics statement

Informed written consent in accordance with the Institutional guidelines (protocol approved by the Ethics Committee of Clinical Research of the Faculty of Biology and Medicine, University of Lausanne, Switzerland) was obtained for all subjects included in the LAU dataset.

The HCP imaging data in this study are from the data sample labeled 100 Unrelated Subjects in ConnectomeDB (https://db.humanconnectome.org), the database managed by the Washington University-University of Minnesota (WU-Minn) consortium of the Human Connectome Project (HCP; http://www.humanconnectome.org). Participants were recruited by the WU-Minn HCP consortium and provided written informed consent prior to experiments [35]. All experimental procedures were approved by the Institutional Review Board (IRB) at Washington University (IRB number 201204036; "Mapping the Human Connectome: Structure, Function, and Heritability") and no further IRB approval is required for our data analysis.

Data sets

LAU. Forty healthy subjects (16 females; 25.3 ± 4.9 years old) underwent an MRI session on a 3T Siemens Trio scanner with a 32-channel head coil. Magnetization prepared rapid acquisition with gradient echo (MPRAGE) sequence was 1-mm in-plane resolution and 1.2-mm slice thickness. DSI sequence included 128 diffusion weighted volumes + 1 reference b0 volume, maximum b value 8000 s/mm^2, and 2.2 × 2.2 × 3.0 mm voxel size. EPI sequence was 3.3-mm in-plane resolution and 3.3-mm slice thickness with TR 1920 ms. DSI and MPRAGE data were processed using the Connectome Mapper Toolkit [59]. Each participant's gray and white matter compartments were segmented from the MPRAGE volume. The grey matter volume was subdivided into 68 cortical and 15 subcortical anatomical regions, according to the Desikan-Killiany atlas, defining 83 anatomical regions. These regions were hierarchically subdivided to obtain five parcellations, corresponding to five different scales [60]. The present study uses a parcellation comprising 233 regions of interest (ROI). Whole brain deterministic streamline tractography was performed on reconstructed DSI data, initiating 32 streamline propagations (seeds) per diffusion direction, per white matter voxel [61]. Within each voxel, seeds were randomly placed and for each seed, a fiber streamline was grown in two opposite directions with a 1mm fixed step. Fibers were stopped if a change in direction was greater than 60 degrees/mm. The process was complete when both ends of the fiber left the white matter mask. For each individual subject, connection weights between pairs of ROI are quantified as a fiber density [62]. Thus, the connection weight between the pair of brain regions $\{u,v\}$ captures the average number of streamlines per unit surface between u and v,

corrected by the average length of the streamlines connecting such brain regions. The aim of these corrections is to control for the variability in cortical region size and the linear bias toward longer streamlines introduced by the tractography algorithm. Fiber densities were used to construct individual subject structural connectivity matrices. Each structural connectivity matrix is then modeled as the adjacency matrix $A = \{a_{ij}\}$ of a graph $G = \{V,G\}$ with nodes $V = \{v_1, \ldots, v_n\}$ representing ROIs, and weighted, undirected edges $E = \{e_1, \ldots, e_m\}$ representing anatomical connections with their fiber densities.

HCP. High-resolution diffusion-weighted (DWI) data from the Human Connectome Project [35] including 173 subjects (Q3 release; males and females mixed, age 22–35 years; imaging parameters: voxel size 1.25 mm isotropic, TR/TE 5520/89.5 ms, 90 diffusion directions with diffusion weighting 1000, 2000, or 3000 s/mm^2) was used to reconstruct macroscale human connectomes for each subject. DWI data processing included the following: (1) eddy current and susceptibility distortion correction, (2) reconstruction of the voxelwise diffusion profile using generalized q-sampling imaging, and (3) whole-brain streamline tractography (see ref [63] for details). Cortical segmentation and parcellation was performed on the basis of a high-resolution T1-weighted image (voxel size: 0.7 mm isotropic) using FreeSurfer [64], automatically parcellating the complete cortical sheet into 219 distinct regions using a subdivision of the Desikan-Killiany atlas. White matter pathways were reconstructed using generalized Q-sampling imaging (GQI), and streamline tractography [61]. A streamline was started in each white matter voxel, following the most matching diffusion direction from voxel to voxel until a streamline reached the gray matter, exited the brain tissue, made a turn of >45 degrees or reached a voxel with a low fractional anisotropy (<0.1). For each individual subject, a 219 x 219 weighted connectivity matrix was constructed by taking the strength of reconstructed region-to-region connections as the number of tractography streamlines between i and j, and dividing by the average cortical surface area of both regions [62].

Defining topological distances for weighted human structural connectivity networks

The edge weights of human brain structural connectivity networks are normally defined in terms of proximity measures such as the number of streamlines or fiber densities. These proximity edge-weights are often interpreted as a measure of information flow or traffic capacity that can travel through a connection (a notion that is analogous to the concept of bandwidth in telecommunication networks). Hence, the proximity between two brain regions is determined by the sequence of edges that maximize the traffic or flow capacity. In order to define topological distances on human brain structural connectivity networks, a proximity-to-distance mapping must be applied over the set of edge-weights, such that large edge-weights (large edge-proximities) are mapped onto small edge-distances, and small edge-weights are mapped onto large edge-distances. The proximity-to-distance mapping can be defined in various ways. Following previous work [6,47], in this study we use the mapping $d_{ij} = \log(1/w_{ij})$, where w_{ij} are edge-proximities (i.e. fiber densities) and d_{ij} are the resulting edge-distances. This mapping has been shown to be less biased towards using only a small set of strong connections for shortest paths [6], and moreover, it yields edge-distances with a log-normal distribution, which is consistent with evidence showing log-normal distributions of synaptic strengths between cortical cells [65] and cortico-cortical projections [66]. Finally, in order to implement this mapping, we first normalize all edge-weights, to ensure that w_{ij} are bounded in the interval [0,1]. As shown previously [32], there is a unique linear function that can

normalize any weighted graph onto the unit interval without affecting network properties:

$$\bar{w}_{ij} = \frac{(1-2\epsilon)w_{ij} + (2\epsilon - 1)\cdot MIN(w_{ij})}{MAX(w_{ij}) - MIN(w_{ij})} + \epsilon \tag{2}$$

Here we use $\epsilon = MIN(w_{ij})$, in order to obtain normalized edge-weights in the interval (0,1) which allows us to apply the proximity-to-distance map $d_{ij} = \log(1/\bar{w}_{ij})$.

Computation of n^t_λ

Let $\mathbf{M} = \{\mathbf{S}, \mathbf{P}_\lambda\}$ be a Markov chain composed by a set of N states $\mathbf{S} = \{1,2,\ldots,N\}$ that correspond element by element to the set of nodes of a graph $\boldsymbol{G}$ with N nodes and E edges; $\mathbf{P}_\lambda$ is the matrix of transition probabilities characterizing the probability of transitioning from one state to another. Then, $\mathbf{P}_\lambda(i,j) \neq 0$ if and only if an edge exists between nodes i and j in graph $\boldsymbol{G}$.

Let $\mathbf{X}$ be a random variable indicating the current state of the chain, or equivalently, the current node where the walker is located; $\mathbf{Y}$ is the random variable indicating the node to which the walker will move in the next time step, and $\mathbf{T}$ is the random variable indicating the target node where the walk will terminate (we assume that $\mathbf{M}$ is an irreducible chain). For a given value of λ, and an specified target $\mathbf{T} = t$, let $\mathbf{P}_\lambda$ be the NxN matrix of transition probabilities where elements of $\mathbf{P}_\lambda$ are defined as

$$P_\lambda(Y = j|X = i, T = t) = \exp(-(\lambda(d_{ij} + g_{jt}) + d_{ij}))\frac{1}{Z_i^t} \tag{3}$$

where $Z_i^t = \sum_j \exp(-(\lambda(d_{ij} + g_{jt}) + d_{ij}))$ is a normalization factor, d_{ij} is the distance from i to j and g_{jt} is the geodesic distance from j to the target node t.

We make $\mathbf{M}$ an absorbing chain and t an absorbing state by setting all transition probabilities $\mathrm{P}_\lambda(\mathbf{Y} = j|\mathbf{X} = t,\mathbf{T} = t) = 0$ for $j \neq t$ and $\mathrm{P}_\lambda(\mathbf{Y} = j|\mathbf{X} = t,\mathbf{T} = t) = 1$ for $j = t$, and define $\mathbf{Q}^t{}_\lambda$ as the $(N\text{-}1)$x$(N\text{-}1)$ matrix of transition probabilities from non-absorbing to non-absorbing states. Then, $\mathbf{n}^t_\lambda = (\mathrm{I}\text{-}\ \mathbf{Q}^t{}_\lambda)^{-1}$ is the fundamental matrix for the absorbing chain [67], and the elements $\mathrm{n}^t{}_\lambda(i,j)$ denote the amount of time that the chain spends in the j-th non-absorbing state when the chain is initialized in the i-th non-absorbing state. In other words, if we take $\mathbf{P}_\lambda$ to represent the transition probabilities for a (biased) random walker on graph $\boldsymbol{G}$, and going from a source node i to a target node t, then $\mathrm{n}^t{}_\lambda(i,j)$ represents the number of times that the random walker starting at node i visits node j before it reaches node t.

Transition probabilities for degenerate paths

Let π_1 and π_2 be any two paths going from node i to node t through edges $\{i,j\}$, and $\{i,k\}$, respectively. The ratio between the transition probabilities $P^t{}_{ij}$ and $P^t{}_{ik}$ is:

$$\frac{P^t_{ij}}{P^t_{ik}} = \frac{\exp(-\lambda(d_{ij} + g_{jt}))\exp(-d_{ij})}{\exp(-\lambda(d_{ik} + g_{kt}))\exp(-d_{ik})} \tag{4}$$

Assume that the length of π_1 and π_2 is equal, so $d_{ij}+g_{jt} = d_{ik}+g_{kt}$. Then we can write:

$$\frac{P^t_{ij}}{P^t_{ik}} = \frac{\exp(-d_{ij})}{\exp(-d_{ik})} \tag{5}$$

Now, let S indicate the set of edges leaving from node i along which there is a shortest path from node i to node t. Since all edges in S lie on shortest paths, for any pair of edges $\{i,j\},\{i,k\}\in$

S, it must be that $d_{ij}+g_{jt} = d_{ik}+g_{kt}$. Then, when $\lambda \to \infty$, we can write

$$P_{ij}^{t} = \begin{cases} \frac{\exp(-d_{ij})}{\sum_{\{i,j'\}\in S}\exp(-d_{ij'})} & if\ \{i,j\} \in S \\ 0 & otherwise \end{cases} \quad (6)$$

If the network is unweighted, then all d_{ij} = const. In that case, all edges in S will have a uniform transition probability from node i.

Note that in the $\lambda \to \infty$ case, only transitions along shortest paths will be allowed. This means that the random walk path lengths will be equal to shortest path lengths.

Randomized networks

For each subject, we created a population of 500 randomized brain networks, with preserved degree and strength sequence, and preserved weight distribution, following the procedure described in [68], which is a modified version of the randomizations proposed in [69,70]. Specifically, the empirical networks were first binarized and then randomized by swapping pairs of connections as proposed by Maslov and Sneppen in [71], thus preserving the binary degree of each node. In order to approximate the strength sequence of the empirical structural connectivity matrices, we shuffle the empirical weights and randomly assign them to the edges of the randomized network. Then, we used a simulated annealing algorithm that minimizes the cost function $C = \Sigma_i|s_i—r_i|$, where s_i is the strength of node i in the empirical network and r_i is the strength in the randomized network. The cost function is minimized by randomly permuting weight assignments across edges and probabilistically accepting the permutations that reduced the energy as the temperature parameter of the algorithm is decreased. The annealing schedule consisted of 123 iterations and a starting temperature of $t_0 = 100$, which was scaled by 0.125 after each iteration. The result of this procedure was an average final energy of $C = 0.2797 \pm 0.04$, which indicates that the average strength discrepancy per node was between 0.0011–0.0014.

Intrinsic connectivity networks

We mapped the Desikan Killiany anatomical parcels used to construct individual subject structural connectivity networks, onto the seven intrinsic connectivity networks (ICN) defined by Yeo et al. (2011) [72]. This parcellation was derived by using a clustering algorithm to partition the cerebral cortex of 1000 healthy subjects into networks of functionally coupled regions. The clustering procedure resulted in the definition of seven clusters comprising systems previously described in the literature including the visual (VIS) and somatomotor (SM) regions, dorsal (DA) and ventral (VA) attention networks, frontoparietal control (FP), limbic (LIM) and default mode network (DMN). The mapping between the Desikan-Killiany anatomical parcels and the seven ICNs from the ICN parcellation was obtained by extracting the vertices of the brain surface corresponding to each anatomical region in the Desikan-Killiany atlas, and then evaluating the mode of the vertices' assignment in the ICN parcellation.

Supporting information

S1 Fig. A spectrum of communication processes.
(PDF)

S2 Fig. Nodal average transmission costs for four increasingly biased routing strategies.
(PDF)

S3 Fig. A brain region's propensity to be a costly source or target.
(PDF)

S4 Fig. Network average values of C_{λ}^{trans} (left panel) and C_{λ}^{info} (middle panel) as a function of λ.
(PDF)

S5 Fig. Communication cost trade-off within subjects.
(PDF)

S6 Fig. z-scored source transmission costs as a function of λ.
(PDF)

S7 Fig. z-scored target transmission costs as a function of λ.
(PDF)

S8 Fig. z-scored source informational costs as a function of λ.
(PDF)

S9 Fig. z-scored target informational costs as a function of λ.
(PDF)

S1 Text. Comparison between the nodal C_{λ}^{trans} measures ($\overrightarrow{C}_{\lambda}^{trans}$ and $\overleftarrow{C}_{\lambda}^{trans}$) and communicability, betweenness centrality, page rank centrality and clustering coefficient.
(PDF)

S2 Text. Testing the effect of binarizing the structural connectivity networks.
(PDF)

Acknowledgments

The authors thank Alessandra Griffa for providing the processed DTI data as well as computational tools for visualization. We also thank Filip Miscevic and Bratislav Mišić for fruitful discussions.

Author Contributions

Conceptualization: Andrea Avena-Koenigsberger, Artemy Kolchinsky, Olaf Sporns.

Data curation: Martijn P. van den Heuvel, Patric Hagmann.

Formal analysis: Andrea Avena-Koenigsberger, Xiaoran Yan, Artemy Kolchinsky, Olaf Sporns.

Supervision: Olaf Sporns.

Writing – original draft: Andrea Avena-Koenigsberger, Artemy Kolchinsky, Olaf Sporns.

Writing – review & editing: Andrea Avena-Koenigsberger, Xiaoran Yan, Artemy Kolchinsky, Martijn P. van den Heuvel, Patric Hagmann, Olaf Sporns.

References

1. Laughlin S.B., & Sejnowski T.J. Communication in neuronal networks. *Science* 301, 1870–1874 (2003) https://doi.org/10.1126/science.1089662 PMID: 14512617
2. Hu Y., Wang Y., Li D., Havlin S., & Di Z. Possible origin of efficient navigation in small worlds. *Physical Review Letters*, 106(10), 108701 (2011) https://doi.org/10.1103/PhysRevLett.106.108701 PMID: 21469842

3. Kleinberg J. M. Navigation in a small world. *Nature*, 406(6798), 845–845 (2000) https://doi.org/10.1038/35022643 PMID: 10972276
4. Crucitti P., Latora V., Marchiori M., & Rapisarda A. Efficiency of scale-free networks: error and attack tolerance. *Physica A*: *Statistical Mechanics and its Applications*, 320, 622–642 (2003)
5. Kalavri V., Simas T., & Logothetis D. The shortest path is not always a straight line: leveraging semi-metricity in graph analysis. *Proceedings of the VLDB Endowment*, 9(9), 672–683 (2016)
6. Avena-Koenigsberger A., Mišić B., Hawkins R. X., Griffa A., Hagmann P., Goñi J., & Sporns O. Path ensembles and a tradeoff between communication efficiency and resilience in the human connectome. *Brain Structure and Function*, 222(1), 603–618 (2017) https://doi.org/10.1007/s00429-016-1238-5 PMID: 27334341
7. Yan G., Zhou T., Hu B., Fu Z. Q., & Wang B. H. Efficient routing on complex networks. *Physical Review E*, 73(4), 046108 (2006)
8. Yu H., Kim P. M., Sprecher E., Trifonov V., & Gerstein M. The importance of bottlenecks in protein networks: correlation with gene essentiality and expression dynamics. *PLoS Comput Biol*, 3(4), e59 (2007) https://doi.org/10.1371/journal.pcbi.0030059 PMID: 17447836
9. Tombu M.N., Asplund C.L., Dux P.E., Godwin D., Martin J.W., & Marois R. A unified attentional bottleneck in the human brain. *Proceedings of the National Academy of Sciences*, 108(33), 13426–13431 (2011)
10. Dodds P. S., Watts D. J., & Sabel C. F. Information exchange and the robustness of organizational networks. *c*, 100(21), 12516–12521 (2003)
11. Boccaletti S., Latora V., Moreno Y., Chavez M., & Hwang D. U. Complex networks: Structure and dynamics. *Physics reports*, 424(4), 175–308 (2006)
12. Goñi J., et al. Exploring the morphospace of communication efficiency in complex networks. *PLoS One*, 8(3), e58070 (2013) https://doi.org/10.1371/journal.pone.0058070 PMID: 23505455
13. Chen B. L., Hall D. H., & Chklovskii D. B. Wiring optimization can relate neuronal structure and function. *Proceedings of the National Academy of Sciences of the United States of America*, 103(12), 4723–4728 (2006) https://doi.org/10.1073/pnas.0506806103 PMID: 16537428
14. Barthélemy M. Spatial networks. *Physics Reports*, 499(1), 1–101 (2011)
15. Bullmore E., & Sporns O. The economy of brain network organization. *Nature Reviews Neuroscience*, 13(5), 336–349 (2012) https://doi.org/10.1038/nrn3214 PMID: 22498897
16. Clune J., Mouret J.B. & Lipson H. The evolutionary origins of modularity. *Proc. R. Soc. B*, 280(1755), p.20122863 (2013) https://doi.org/10.1098/rspb.2012.2863 PMID: 23363632
17. Betzel R.F., et al. Generative models of the human connectome. *Neuroimage*, 124, pp.1054–1064 (2016) https://doi.org/10.1016/j.neuroimage.2015.09.041 PMID: 26427642
18. Noh J. D., & Rieger H. Random walks on complex networks. *Physical review letters*, 92(11), 118701 (2004) https://doi.org/10.1103/PhysRevLett.92.118701 PMID: 15089179
19. Yang S. J. Exploring complex networks by walking on them. *Physical Review E*, 71(1), 016107 (2005)
20. Tejedor V., Bénichou O., & Voituriez R. Global mean first-passage times of random walks on complex networks. *Physical Review E*, 80(6), 065104 (2009)
21. Masuda N., Porter M.A. and Lambiotte R. Random walks and diffusion on networks. *Physics Reports*. (2017)
22. Adamic L. A., Lukose R. M., Puniyani A. R., & Huberman B. A. Search in power-law networks. *Physical review E*, 64(4), 046135 (2001)
23. Yin C. Y., Wang B. H., Wang W. X., Zhou T., & Yang H. J. Efficient routing on scale-free networks based on local information. *Physics letters A*, 351(4), 220–224 (2006)
24. van den Heuvel M. P., Kahn R. S., Goñi J., & Sporns O. High-cost, high-capacity backbone for global brain communication. *Proceedings of the National Academy of Sciences*, 109(28), 11372–11377 (2012)
25. Csoma A., et al. Routes Obey Hierarchy in Complex Networks. *Scientific reports*, 7(1), p.7243. (2017) https://doi.org/10.1038/s41598-017-07412-4 PMID: 28775278
26. Fronczak A., & Fronczak P. Biased random walks in complex networks: The role of local navigation rules. *Physical Review E*, 80(1), 016107 (2009)
27. Lambiotte R., Sinatra R., Delvenne J. C., Evans T. S., Barahona M., & Latora V. Flow graphs: Interweaving dynamics and structure. *Physical Review E*, 84(1), 017102 (2011)
28. Zlatić V., Gabrielli A., & Caldarelli G. Topologically biased random walk and community finding in networks. *Physical Review E*, 82(6), 066109 (2010)
29. Boguna M., Krioukov D., & Claffy K.C. Navigability of complex network. *Nat Phys* 5(1) 74–80 (2009)

30. Simsek O., Jensen D. Navigating networks by using homophily and degree. *Proceedings of the National Academy of Sciences* USA 105(35) 12758–12762 (2008)
31. Yan X., Teng S.H., Lerman K. and Ghosh R. Capturing the interplay of dynamics and networks through parameterizations of Laplacian operators. *PeerJ Computer Science*, 2, p.e57. (2016)
32. Simas T., Chavez M., Rodriguez P.R. and Diaz-Guilera A. An algebraic topological method for multimodal brain networks comparisons. *Frontiers in psychology*, 6, p.904 (2015) https://doi.org/10.3389/fpsyg.2015.00904 PMID: 26217258
33. Simas T., & Rocha L.M. Distance closures on complex networks. *Network Science*, 3(02), 227–268 (2015)
34. Todorov E. Efficient computation of optimal actions. *Proceedings of the national academy of sciences*, 106(28), 11478–11483 (2009)
35. Van Essen D.C., et al. The WU-Minn Human Connectome Project: an overview. Neuroimage 80:6279 (2013)
36. Glasser M.F., et al.The minimal preprocessing pipelines for the human connectome project Neuro-Image, 80, 105–124 (2013) https://doi.org/10.1016/j.neuroimage.2013.04.127 PMID: 23668970
37. Avena-Koenigsberger A.,et al. Using Pareto optimality to explore the topology and dynamics of the human connectome. *Phil. Trans. R. Soc. B*, 369(1653), 20130530 (2014)
38. Page L., Brin S., Motwani R., & Winograd T. *The PageRank citation ranking: Bringing order to the web*. Stanford InfoLab (1999)
39. Estrada E. and Hatano N. Communicability in complex networks. *Physical Review E*, 77(3), p.036111 (2008)
40. Avena-Koenigsberger A., Mišić B., & Sporns O. Communication Dynamics. *Nature Review Neuroscience* 19, 17–33 (2018)
41. Roland P.E., Hilgetag C.C., & Deco G. Cortico-cortical communication dynamics. *Frontiers in systems neuroscience*, 8 (2014)
42. Fries P. Rhythms for cognition: communication through coherence. *Neuron*, 88(1), 220–235 (2015) https://doi.org/10.1016/j.neuron.2015.09.034 PMID: 26447583
43. Palmigiano A., Geisel T., Wolf F., & Battaglia D. Flexible information routing by transient synchrony. *Nature Neuroscience* 20(7), 1014 (2017) https://doi.org/10.1038/nn.4569 PMID: 28530664
44. Latora V., & Marchiori M. Efficient behavior of small-world networks. *Physical Review Letters*, 87(19), 198701 (2001) https://doi.org/10.1103/PhysRevLett.87.198701 PMID: 11690461
45. Humphries M. D., & Gurney K. Network 'small-world-ness': a quantitative method for determining canonical network equivalence. *PloS one*, 3(4), e0002051 (2008) https://doi.org/10.1371/journal.pone.0002051 PMID: 18446219
46. Van Wijk B.C., Stam C.J., & Daffertshofer A. Comparing brain networks of different size and connectivity density using graph theory. *PloS one*, 5(10), e13701 (2010) https://doi.org/10.1371/journal.pone.0013701 PMID: 21060892
47. Goñi J., et al. Resting-brain functional connectivity predicted by analytic measures of network communication. *Proceedings of the National Academy of Sciences*, 111(2), 833–838 (2014)
48. Stam C. J., & van Straaten E. C. Go with the flow: use of a directed phase lag index (dPLI) to characterize patterns of phase relations in a large-scale model of brain dynamics. *Neuroimage*, 62(3), 1415–1428 (2012) https://doi.org/10.1016/j.neuroimage.2012.05.050 PMID: 22634858
49. Moon J. Y., Lee U., Blain-Moraes S., & Mashour G. A. General relationship of global topology, local dynamics, and directionality in large-scale brain networks. *PLoS computational biology*, 11(4), e1004225 (2015) https://doi.org/10.1371/journal.pcbi.1004225 PMID: 25874700
50. Delvenne J.C., Schaub M.T., Yaliraki S.N., & Barahona M. The stability of a graph partition: A dynamics-based framework for community detection. In *Dynamics On and Of Complex Networks*, *Volume* 2 (pp. 221–242). Springer New York (2013)
51. Bertolero M.A., Yeo B.T., & D'Esposito M. The Diverse Club: The Integrative Core of Complex Networks. *Nature Communications* 8; 1277 (2017) https://doi.org/10.1038/s41467-017-01189-w PMID: 29097714
52. Bertolero M.A., Yeo B.T., & D'Esposito M. The modular and integrative functional architecture of the human brain. *Proceedings of the National Academy of Sciences*, 112(49), E6798–E6807. (2015)
53. Barbey, Aron K. Network neuroscience theory of human intelligence. *Trends in cognitive sciences*, 22.1, 8–20 (2018). https://doi.org/10.1016/j.tics.2017.10.001 PMID: 29167088
54. Guimerà R., Díaz-Guilera A., Vega-Redondo F., Cabrales A. and Arenas A., Optimal network topologies for local search with congestion. *Physical review letters*, 89(24), p.248701 (2002). https://doi.org/10.1103/PhysRevLett.89.248701 PMID: 12484988

55. Françoisse K., Kivimäki I., Mantrach A., Rossi F. and Saerens M. A bag-of-paths framework for network data analysis. *Neural Networks*, 90, pp.90–111 (2017) https://doi.org/10.1016/j.neunet.2017.03.010 PMID: 28458082

56. Mišić B., Sporns O., & McIntosh A.R. Communication Efficiency and Congestion of Signal Traffic in Large-Scale Brain Networks. *PLoS Comput Biol* 10(1): e1003427 (2014) https://doi.org/10.1371/journal.pcbi.1003427 PMID: 24415931

57. Betzel R.F., & Bassett D.S. Multi-scale brain networks. *Neuroimage* 160,73–83(2016) https://doi.org/10.1016/j.neuroimage.2016.11.006 PMID: 27845257

58. Messé A., Rudrauf D., Giron A. and Marrelec G. Predicting functional connectivity from structural connectivity via computational models using MRI: an extensive comparison study. *NeuroImage* 111, pp.65–75 (2015) https://doi.org/10.1016/j.neuroimage.2015.02.001 PMID: 25682944

59. Daducci A., et al. The connectome mapper: an open-source processing pipeline to map connectomes with MRI. *PloS one*, 7(12), e48121 (2012) https://doi.org/10.1371/journal.pone.0048121 PMID: 23272041

60. Cammoun L., et al. Mapping the human connectome at multiple scales with diffusion spectrum MRI. *Journal of neuroscience methods*, 203(2), 386–397 (2012) https://doi.org/10.1016/j.jneumeth.2011.09.031 PMID: 22001222

61. Wedeen V.J., et al. Diffusion spectrum magnetic resonance imaging (DSI) tractography of crossing fibers. *Neuroimage*, 41(4), 1267–1277 (2008) https://doi.org/10.1016/j.neuroimage.2008.03.036 PMID: 18495497

62. Hagmann P., et al. Mapping the structural core of human cerebral cortex. *PLoS Biol*, 6(7), e159 (2008) https://doi.org/10.1371/journal.pbio.0060159 PMID: 18597554

63. de Reus M.A., van den Heuvel M.P. Simulated rich club lesioning in brain networks: a scaffold for communication and integration? Front Hum Neurosci 8:647, https://doi.org/10.3389/fnhum.2014.00647 PMID: 25191259 (2014)

64. Fischl B., et al. Automatically parcellating the human cerebral cortex. Cereb Cortex 14:11–22, https://doi.org/10.1093/cercor/bhg087 PMID: 14654453 (2004)

65. Buzsaki G., & Mizuseki K. The log-dynamic brain: how skewed distributions affect network operations. Nat Rev Neurosci 15(4):264–278 (2014) https://doi.org/10.1038/nrn3687 PMID: 24569488

66. Markov N.T., et al. A weighted and directed interareal connectivity matrix for macaque cerebral cortex. Cereb Cortex. 270 (2012)

67. Grinstead C.M., & Snell J.L. Introduction to Probability 2nd edn (Providence, RI: American Mathematical Society) (2003)

68. Mišić B., et al. Cooperative and competitive spreading dynamics on the human connectome. *Neuron*, 86(6), 1518–1529 (2015) https://doi.org/10.1016/j.neuron.2015.05.035 PMID: 26087168

69. Opsahl T., Colizza V., Panzarasa P., & Ramasco J.J. Prominence and control: the weighted rich-club effect. *Physical review letters*, 101(16), 168702. (2008) https://doi.org/10.1103/PhysRevLett.101.168702 PMID: 18999722

70. Zlatic, et al. On the rich-club effect in dense and weighted networks. *The European Physical Journal B*, 67(3), 271–275 (2009)

71. Maslov S., & Sneppen K. Specificity and stability in topology of protein networks. *Science*, 296(5569), 910–913 (2002) https://doi.org/10.1126/science.1065103 PMID: 11988575

72. Yeo B.T., et al. The organization of the human cerebral cortex estimated by intrinsic functional connectivity. J Neurophysiol 106(3):1125–1165 (2011) https://doi.org/10.1152/jn.00338.2011 PMID: 21653723